Least Square-based Finite Volumes for Solving the Advection-Diffusion of Contaminants in Porous Media

Enrico Bertolazzi[1] **Gianmarco Manzini**[2]

[1]Dipartimento di Ingegneria Meccanica e Strutturale,
Università di Trento, via Mesiano 77, I – 38050 Trento, Italy
enrico.bertolazzi@ing.unitn.it

[2]Istituto di Matematica Applicata e Tecnologie Informatiche,
CNR, via Ferrata 1, I – 27100 Pavia, Italy
marco.manzini@imati.cnr.it

Abstract

A 2-nd order cell-centered Finite-Volume method is proposed to solve the steady advection-diffusion equation for contaminant transport in porous media. This method is based on a linear least square reconstruction that maintains the approximate cell-average values. The reconstruction is combined with an appropriate slope limiter to prevent the formation of spurious oscillations in the convection-dominated case. The theoretical convergence rate is investigated on a boundary layer problem, and the preliminar results show that the method is promising in the numerical simulation of more complex groundwater flow problems.

Keywords: Finite Volume, non-oscillatory reconstructions, limiters.

1. Introduction

The process of groundwater transport of a solute in porous media is usually captured by mathematical models based on the advection-diffusion equation. The numerical approximation of transport phenomenon can be quite difficult because of the advective term. When the advection effects are dominant on the diffusive ones, sharp fronts of solute concentration can form and move throughout the computational domain. It is a well-known fact that in such a situation,

spurious $\mathcal{O}(1)$ non-physical oscillations known as Gibbs' phenomena, can develop and deteriorate the accuracy of the numerical solution obtained using standard finite difference and finite element methods. To overcome the process of oscillation formation and ensure a type of numerical stability with minimal artificial diffusion, shock-capturing numerical schemes have been developed and widely investigate in the last two decades [1]. Many schemes are thus based on the splitting of the advection and the diffusion terms into two separate partial differential equations, and in this context, the coupling of quite different methods, such as Finite Volumes and Finite Elements, is not unusual: let us mention the Eulerian-Lagrangian schemes [2, 3] and the fully Eulerian Godunov mixed methods [4, 5, 6]. In almost all of the aforementioned methods, time-explicit, spatially second-order accurate Godunov method is basically used to treat advection, and a time-implicit, spatially second-order accurate mixed finite element method is used for modeling the diffusion.

The numerical schemes that is investigated in this work is instead based on a Finite Volume discretization of both the advective and the diffusive flux. The advective term is approximated using an upstream technique, while a central scheme is applied to the diffusion one. The second-order accuracy is formally achieved by employing a linear reconstruction that maintains the approximate cell-average values computed by the scheme. The stability of the scheme is ensured by an appropriate slope limiter combined with the reconstruction.

2. Advective and Diffusive Transport

Let Ω a connected polygonal domain in $\mathbb{R}^2$ defined by a closed (1-D) surface $\partial\Omega$. The governing equation of the phenomenon we are interested in reads as

$$\nabla \cdot (\mathbf{V}C - D\nabla C) = S \quad \text{in} \quad \Omega. \tag{1}$$

Equation (1) describes the steady advective-diffusive transport of a contaminant whose spatial concentration distribution is denoted by $C(\mathbf{x})$. The contaminant is passively advected by $\mathbf{V}(\mathbf{x})$, which is an assigned convection field; $D(\mathbf{x})$ is the diffusion tensor, and $S(t, \mathbf{x})$ is the contaminant production/consumption source term [7].

The border $\partial\Omega$ may be partitioned into the union of two non-overlapping and possibly empty subsets, Γ_D and Γ_N, where respectively Dirichlet and Neumann boundary conditions are specified: $\partial\Omega = \Gamma_D \cup \Gamma_N$. The boundary conditions are given by

$$\begin{aligned} &\text{Dirichlet}: && C = \mathsf{g_d} && \text{on} \quad \Gamma_D, \\ &\text{Neumann}: && -D\nabla C \cdot \mathbf{n} = \mathsf{g_n} && \text{on} \quad \Gamma_N, \end{aligned} \tag{2}$$

where $\mathsf{g_d}$ and $\mathsf{g_n}$ are assumed to be smooth functions.

3. The Finite Volume Formulation

The design of our FV method starts as usual by reformulating in an integral form the model problem defined by equations (1) and (2) on a set of closed and non-overlapping control volumes $\mathsf{T}_i \in \mathcal{T}_h$, where $\mathcal{T}_h$ is a conformal triangulation of Ω [8]. Integrating equation (1) over T_i, applying the Gauss divergence theorem and imposing when required the boundary conditions given in (2), we have

$$\begin{aligned} &\sum_{j\in\mathcal{T}_h(i)} \int_{\mathsf{e}_{ij}} \Big[C(\mathbf{x})\mathbf{V}(\mathbf{x}) - D(\mathbf{x})\nabla C(\mathbf{x}) \Big] \cdot \mathbf{n}_{ij}\, d\ell + \\ &\sum_{j'\in\mathcal{T}_h^d(i)} \int_{\mathsf{e}_{ij}} \mathsf{g}_\mathsf{d}(\mathbf{x})\mathbf{V}(\mathbf{x}) \cdot \mathbf{n}_{ij}\, d\ell - \sum_{j'\in\mathcal{T}_h^n(i)} \int_{\mathsf{e}_{ij}} \mathsf{g}_\mathsf{n}(\mathbf{x})\, d\ell = \int_{\mathsf{T}_i} S(\mathbf{x}, C)\, d\mathbf{x}, \end{aligned} \tag{3}$$

for every $\mathsf{T}_i \in \mathcal{T}_h$. In (3) $\mathcal{T}_h(i)$ is the index set of volumes adjacent to T_i, e_{ij} is the edge shared by T_i and T_j, i.e. $\mathsf{e}_{ij} = \mathsf{T}_i \cap \mathsf{T}_j$. $\mathcal{T}_h^d(i)$ and $\mathcal{T}_h^n(i)$ are the index set of the edges of T_i located on the domain boundary, i.e. $\mathsf{e}_{ij} = \mathsf{T}_i \cap \Gamma_D$ and $\mathsf{e}_{ij} = \mathsf{T}_i \cap \Gamma_N$ respectively. The symbol $\mathbf{n}_{ij}$ stands for the vector that is normal to the edge e_{ij} and oriented from T_i to T_j when the edge is internal, or outward-directed when the edge is on the boundary.

The Finite Volume method is formulated on each volumes $\mathsf{T}_i \in \mathcal{T}_h$ by the equation

$$\sum_{j\in\mathcal{T}_h(i)} \Big[\underbrace{\mathrm{G}_{ij}(\mathbf{c})}_{\text{convection}} + \underbrace{\mathrm{H}_{ij}(\mathbf{c})}_{\text{diffusion}} \Big] + \sum_{j\in\mathcal{T}_h'(i)} \underbrace{\mathrm{F}_{ij'}(\mathbf{c})}_{\text{boundary}} = \underbrace{S_i(\mathbf{c})}_{\text{source}}, \tag{4}$$

where we indicate the numerical flux integral terms corresponding to the ones in (3). The source term $S_i(\mathbf{c})$ is numerically discretized in every cell $\mathsf{T}_i \in \mathcal{T}_h$ by a second-order quadrature formula.

The cell-wise linear approximation to the solution of (1) is defined within T_i by $\widetilde{c_i}(\mathbf{x}) = c_i + \widetilde{\mathcal{G}_i}(\mathbf{c}) \cdot (\mathbf{x} - \mathbf{x}_i)$ for any $\mathbf{x} \in \mathsf{T}_i$ where $\widetilde{\mathcal{G}_i}(\mathbf{c})$ is an $\mathcal{O}(h)$ cell-centered estimate of the solution gradient. The diffusive flux contribution $\mathrm{H}_{ij}(\mathbf{c})$ also requires that an $\mathcal{O}(h)$ edge-centered gradient $\widetilde{\mathcal{G}_{ij}}(\mathbf{c})$ be estimated for each edge e_{ij}. Cell-centered and edge-centered gradients are necessarily reconstructed using the only information available from the scheme, that is the approximate cell averages $\mathbf{c}$, as follows.

First, we apply the Least Square method to approximate solution values at mesh vertices. For any vertex of position $\mathbf{x}_\alpha$, the least square method yields the vertex value c_α in the form of a weighted average of the centroid values c_i taken from the triangles incident to α

$$c_\alpha = \sum_{j\in\mathcal{V}_h(\alpha)} w_j^\alpha\, c_j, \tag{5}$$

where a suitable set of weights $\{w_{\alpha j}\}$ has been introduced.

Then, we apply the Gauss-Green theorem to a closed integration path, which is the cell boundary $\partial \mathsf{T}_i$ for $\widetilde{\mathcal{G}_i}(\mathbf{c})$ and the triangle defined by the centroid of T_i and the vertices of the edge e_{ij} for $\widetilde{\mathcal{G}_i}(\mathbf{c})$.

The gradient approximation is thus determined by using the FV cell average in T_i together with the ones within the surrounding cells and is finally constrained by a special limiting algorithm. The limiter is introduced to control the numerical oscillations that can appear in the approximation process. Further details about these issues are described in Reference [9].

3.1. Limited Gradient Reconstruction and Discretization of the Advection Term

The piecewise-constant gradient $\widetilde{\mathcal{G}_i}(\mathbf{c})$ within the cell T_i is recovered by using the formula

$$\widetilde{\mathcal{G}_i}(\mathbf{c}) = \ell_i \frac{1}{2\,|\mathsf{T}_i|}\mathbf{R}\Big[c_\alpha(\mathbf{x}_\beta - \mathbf{x}_\gamma) + c_\beta(\mathbf{x}_\gamma - \mathbf{x}_\alpha) + c_\gamma(\mathbf{x}_\alpha - \mathbf{x}_\beta)\Big].$$

This gradient is such that the vector $(\widetilde{\mathcal{G}_i}(\mathbf{c})^T, 1)^T$ is orthogonal to the plane for the 3-D vectors $(\mathbf{x}_\alpha, c_\alpha)$, $(\mathbf{x}_\beta, c_\beta)$ and $(\mathbf{x}_\gamma, c_\gamma)$.

The scalar limiting factor ℓ_i is the largest real number in $[0, 1]$ such that

$$\begin{aligned}
&(i) && \min\{c_i, c_j\} \le \widetilde{c}_i(\cdot, \mathbf{x}_{ij}) \le \max\{c_i, c_j\} && \mathsf{e}_{ij} \in \mathcal{E}_h^I \\
&(ii) && \min\{c_i, \mathsf{g}_{\mathsf{d}ij'}\} \le \widetilde{c}_i(\cdot, \mathbf{x}_{ij'}) \le \max\{c_i, \mathsf{g}_{\mathsf{d}ij'}\} && \mathsf{e}_{ij'} \in \mathcal{E}_h^D \\
&(iii) && \Big(\widetilde{\mathcal{G}_i}(\mathbf{c}) \cdot \mathbf{n}_{ij}\Big) \cdot \mathsf{g}_{\mathsf{n}ij} \ge 0, \qquad \Big|d_{ij}\widetilde{\mathcal{G}_i}(\mathbf{c}) \cdot \mathbf{n}_{ij}\Big| \le \big|\mathsf{g}_{\mathsf{n}ij}\big| && \mathsf{e}_{ij'} \in \mathcal{E}_h^N,
\end{aligned}$$

where in (iii), d_{ij} is the edge-average viscosity

$$d_{ij} = \frac{1}{|\mathsf{e}_{ij}|}\int_{\mathsf{e}_{ij}} D(\cdot, \mathbf{x})\, d\ell. \tag{6}$$

This limiting strategy ensures that the recovered gradient is null when c_i is a local minimum or a local maximum. In this way, the linearly reconstructed solution is monotonized, thus providing also that a TVD stability constraint is satisfied.

The advection term in equation (3) is discretized by using a standard upwind technique. We have

$$\begin{aligned}
\mathrm{G}_{ij}(C) \;&=\; \nu_{ij}^+ \widetilde{c}_i(\mathbf{x}_{ij}) + \nu_{ij}^- \widetilde{c}_j(\mathbf{x}_{ij}) = \nu_{ij}^+ \widetilde{c}_i(\mathbf{x}_{ij}) - \nu_{ji}^+ \widetilde{c}_j(\mathbf{x}_{ij}), \\
&\approx \int_{\mathsf{e}_{ij}} C(\mathbf{x})\mathbf{V}(\mathbf{x}) \cdot \mathbf{n}_{ij}\, d\ell, \qquad j \in \mathcal{T}_h(i),
\end{aligned}$$

where we introduced the edge-average integral of the velocity field and its upwind value

$$\nu_{ij} = \int_{\mathsf{e}_{ij}} \mathbf{V}(\mathbf{x}) \cdot \mathbf{n}_{ij}\, d\ell, \qquad \nu_{ij}^{\pm} = \frac{\nu_{ij} \pm |\nu_{ij}|}{2},$$

and use has been made of the property $\nu_{ij}^{-} = -\nu_{ji}^{+}$.

3.2. Edge-Centered Gradient Reconstruction and Discretization of the Diffusive Term

The gradient reconstruction at each internal edge proceeds throughout the following three steps:

(i) compute $\mathcal{G}_{ij}(\mathbf{c}) = \dfrac{3}{2\,|\mathsf{T}_i|}\mathbf{R}\left[(\mathbf{x}_\beta - \mathbf{x}_i)(c_\alpha - c_i) - (\mathbf{x}_\alpha - \mathbf{x}_i)(c_\beta - c_i)\right],$
so that the vector $(\mathcal{G}_{ij}(\mathbf{c})^T, 1)^T$ is orthogonal to the plane for the 3-D points $(\mathbf{x}_k, c_k)$ with $k = i,\ \alpha,\ \beta$;

(ii) compute $\mathcal{G}_{ji}(\mathbf{c}) = \dfrac{3}{2\,|\mathsf{T}_j|}\mathbf{R}\left[(\mathbf{x}_\alpha - \mathbf{x}_j)(c_\beta - c_j) - (\mathbf{x}_\beta - \mathbf{x}_j)(c_\alpha - c_j)\right],$
so that the vector $(\mathcal{G}_{ij}(\mathbf{c})^T, 1)^T$ is orthogonal to the plane for the 3-D points $(\mathbf{x}_k, c_k)$ with $k = j,\ \alpha,\ \beta$;

(iii) compute the non-linear average between $\mathcal{G}_{ij}(\mathbf{c})$ and $\mathcal{G}_{ji}(\mathbf{c})$

$$\begin{aligned} &\widetilde{\mathcal{G}_{ij}}(\mathbf{c}) = W_{ij}(\mathbf{c})\mathcal{G}_{ij}(\mathbf{c}) + W_{ji}(\mathbf{c})\mathcal{G}_{ji}(\mathbf{c}), \\ &W_{ij}(\mathbf{c}),\ W_{ji}(\mathbf{c}) \geq 0, \qquad W_{ij}(\mathbf{c}) + W_{ji}(\mathbf{c}) = 1, \end{aligned} \tag{7}$$

which is finally taken as the gradient estimate at the edge e_{ij}.

The terms $W_{ij}(\mathbf{c})$ in equation (7) are the scalar weights of the final average. A *non-linear average* can be envisaged as detailed in Reference [9]. Let us first identify the *minimum common contribution* – in a sense that is specified below – to the edge-centered gradients $\mathcal{G}_{ij}$ and $\mathcal{G}_{ji}$ within the cells T_i and T_j and split them as the sum of the common term plus a correction gradient (indicated by the "hat"-symbols)

$$\mathcal{G}_{ij}(\mathbf{c}) = D_{ij}(c_j - c_i)\mathbf{n}_{ij} + \hat{\mathcal{G}}_{ij}.$$

Assuming that $D_{ij} = D_{ji}$, and that the weights are

$$W_{ij}(\mathbf{c}) = \begin{cases} \dfrac{|g_{ji}(\mathbf{c})|}{|g_{ij}(\mathbf{c})| + |g_{ji}(\mathbf{c})|}, & \text{if } |g_{ij}(\mathbf{c})| + |g_{ji}(\mathbf{c})| > 0 \\ 1/2 & \text{if } |g_{ij}(\mathbf{c})| + |g_{ji}(\mathbf{c})| = 0 \end{cases}$$

with $g_{ij}(\mathbf{c}) = \hat{\mathcal{G}}_{ij}(\mathbf{c}) \cdot \mathbf{n}_{ij}$, we obtain a non-linear numerical definition of the edge-centered gradients. In [9], it is shown that this approach yields an FV scheme that satisfies a global maximum principle.

Let us now discuss how the quantity D_{ij}, which dimensionally plays the role of a characteristic grid-dependent numerical diffusion times a characteristic length, is defined. Let $\widetilde{c_{ij}}$ be the linear interpolation of c_α and c_β at the point $\mathbf{x}_{ij} \in \mathsf{e}_{ij}$, orthogonal projection of the centroid $\mathbf{x}_i$ onto e_{ij}

$$\widetilde{c_{ij}} = s_{ij}^{\alpha} c_\alpha + s_{ij}^{\beta} c_\beta,$$

where the non-negative linear interpolation coefficients s_{ij}^{α} and s_{ij}^{β} are such that $s_{ij}^{\alpha} + s_{ij}^{\beta} = 1$.

Using the fact that c_α and c_β are least-square interpolated values and can be written as given in (5) and by identifying the contribution from the cell T_j, we have

$$\begin{aligned}\widetilde{c_{ij}} - c_i \;=\; & (s_{ij}^{\alpha} w_j^{\alpha} + s_{ij}^{\beta} w_j^{\beta})(c_j - c_i) + \\ & s_{ij}^{\alpha} \sum_{k \in \mathcal{V}_h(\alpha)\setminus\{j\}} w_k^{\alpha}(c_k - c_i) + s_{ij}^{\beta} \sum_{k \in \mathcal{V}_h(\beta)\setminus\{j\}} w_k^{\beta}(c_k - c_i).\end{aligned}$$

A similar expression can be written for the cell T_j, thus leading to the definition

$$D_{ij} = D_{ji} = \min\left[\frac{s_{ij}^{\alpha} w_j^{\alpha} + s_{ij}^{\beta} w_j^{\beta}}{h_{ij}}, \frac{s_{ji}^{\alpha} w_i^{\alpha} + s_{ji}^{\beta} w_i^{\beta}}{h_{ji}}\right], \tag{8}$$

where h_{ij} and h_{ji} are the distances of the centroids $\mathbf{x}_i$ and $\mathbf{x}_j$ from the edge e_{ij}.

Taking into account properly the definition of $\widetilde{\mathcal{G}_{ij}}(\mathbf{c})$ given in step *(iii)*, the component of this latter vector orthogonal to e_{ij} can be written as

$$\mathrm{H}_{ij}(\mathbf{c}) = d_{ij}\widetilde{\mathcal{G}_{ij}}(\mathbf{c}) \cdot |\mathsf{e}_{ij}|\, \mathbf{n}_{ij} \qquad \text{for all} \quad \mathsf{e}_{ij} \in \mathcal{E}_h,$$

where d_{ij} is defined in (6) and $h_{ij}(\mathbf{c})$ is a bounded non-negative scalar function of the cell averages $\mathbf{c}$.

3.3. The semi-discrete FV Formulation

In this section we re-formulate the FV scheme (4) in a more compact form. Introducing a suitable definition of the matrix operators $\mathbf{G}$, $\widetilde{\mathbf{G}}(\mathbf{c})$, $\mathbf{H}(\mathbf{c})$, $\mathbf{F}$, $\widetilde{\mathbf{F}}(\mathbf{c})$ and the vectors $\mathbf{f}$, $\widetilde{\mathbf{f}}(\mathbf{c})$ – see [10] for the details – the discrete cell-wise advective and diffusive flux balances can be rewritten as:

$$\begin{aligned}\Big[\mathbf{G}\mathbf{c} - \widetilde{\mathbf{G}}(\mathbf{c})\mathbf{c}\Big]_i &= \sum_{j \in \mathcal{T}_h(i) \cup \mathcal{T}_h'(i)} \mathrm{G}_{ij}(\mathbf{c}), \\ \Big[\mathbf{H}(\mathbf{c})\mathbf{c}\Big]_i &= \sum_{j \in \mathcal{T}_h(i) \cup \mathcal{T}_h'(i)} \mathrm{H}_{ij}(\mathbf{c}),\end{aligned} \tag{9}$$

Table 1: Absolute and relative errors and convergence rates.

$N_X \times N_Y$	$\mathcal{E}^{Abs}$	$\mathcal{E}^{rel}$	Rate	$\widetilde{\mathcal{E}}^{Abs}$	$\widetilde{\mathcal{E}}^{rel}$	Rate
5×5	$2.21\,10^{-3}$	$3.40\,10^{-3}$	—	$2.69\,10^{-3}$	$2.39\,10^{-3}$	—
10×10	$5.59\,10^{-4}$	$8.62\,10^{-4}$	1.98	$7.20\,10^{-4}$	$6.40\,10^{-4}$	1.90
20×20	$1.41\,10^{-4}$	$2.17\,10^{-4}$	1.98	$1.85\,10^{-4}$	$1.64\,10^{-4}$	1.96
40×40	$3.54\,10^{-5}$	$5.45\,10^{-5}$	1.99	$4.66\,10^{-5}$	$4.15\,10^{-5}$	1.98
$D = 1$						
5×5	$4.47\,10^{-3}$	$6.26\,10^{-3}$	—	$6.39\,10^{-3}$	$5.16\,10^{-3}$	—
10×10	$1.15\,10^{-3}$	$1.61\,10^{-3}$	1.95	$1.76\,10^{-3}$	$1.43\,10^{-4}$	1.85
20×20	$2.91\,10^{-4}$	$4.08\,10^{-4}$	1.98	$4.61\,10^{-4}$	$3.73\,10^{-4}$	1.93
40×40	$7.33\,10^{-5}$	$1.03\,10^{-5}$	1.99	$1.17\,10^{-4}$	$9.48\,10^{-5}$	1.97
$D = 0.5$						
5×5	$9.98\,10^{-3}$	$1.23\,10^{-2}$	—	$1.54\,10^{-2}$	$1.10\,10^{-2}$	—
10×10	$2.71\,10^{-3}$	$3.34\,10^{-3}$	1.88	$4.72\,10^{-3}$	$3.36\,10^{-3}$	1.70
20×20	$6.99\,10^{-4}$	$8.62\,10^{-4}$	1.95	$1.29\,10^{-4}$	$9.21\,10^{-4}$	1.86
40×40	$1.77\,10^{-4}$	$2.19\,10^{-5}$	1.98	$3.37\,10^{-5}$	$2.40\,10^{-4}$	1.94
$D = 0.25$						
5×5	$2.91\,10^{-2}$	$3.15\,10^{-2}$	—	$3.13\,10^{-2}$	$1.96\,10^{-2}$	—
10×10	$9.18\,10^{-3}$	$9.96\,10^{-3}$	1.66	$1.41\,10^{-2}$	$8.84\,10^{-3}$	1.15
20×20	$2.58\,10^{-3}$	$2.79\,10^{-3}$	1.83	$4.60\,10^{-3}$	$2.88\,10^{-3}$	1.61
40×40	$6.75\,10^{-4}$	$7.32\,10^{-4}$	1.93	$1.29\,10^{-3}$	$8.10\,10^{-4}$	1.82
40×40	$1.77\,10^{-4}$	$2.19\,10^{-5}$	1.98	$3.37\,10^{-5}$	$2.40\,10^{-4}$	1.94
$D = 0.1$						

while the contribution from boundary edges becomes

$$\left[\mathbf{F}\mathbf{c} - \widetilde{\mathbf{F}}(\mathbf{c})\mathbf{c} - (\mathbf{f} - \widetilde{\mathbf{f}}(\mathbf{c}))\right]_i = \sum_{j \in \mathcal{T}_h'(i)} \mathrm{F}_{ij}(\mathbf{c}). \tag{10}$$

The r.h.s. source is denoted by the symbol $\mathbf{S}(\mathbf{c})$. Using the definitions (9) and (10) the final matrix-vector form is obtained for the FV scheme (4)

$$\mathbf{N}(\mathbf{c})\mathbf{c} = \widetilde{\mathbf{N}}(\mathbf{c})\mathbf{c} + \mathbf{b}(\mathbf{c}). \tag{11}$$

In equation (11), the term $\mathbf{b}(\mathbf{c}) = \mathbf{f} - \widetilde{\mathbf{f}}(\mathbf{c}) + \mathbf{b}^S(\mathbf{c})$ collects all of the contributions from the boundary edge fluxes. We have also introduced the non-linear matrix operators $\mathbf{N}(\mathbf{c}) = \mathbf{F} + \mathbf{G} + \mathbf{H}(\mathbf{c}) + \mathbf{A}(\mathbf{c})$ and $\widetilde{\mathbf{N}}(\mathbf{c}) = \widetilde{\mathbf{F}}(\mathbf{c}) + \widetilde{\mathbf{G}}(\mathbf{c})$.

4. Numerical Results

In this section a set of numerical results is shown on the following test case to illustrate experimentally both the accuracy of the proposed method and its

shock-capturing capabilities.

The contaminant concentration C is advected within the domain $\Omega = [0,\, 1] \times [0,\, 1]$ by a constant velocity field $\mathbf{V} = (1, 0)$ and homogeneously and isotropically diffused by a constant viscosity D which takes values in the range $[10^{-4}, 1]$.

The boundary conditions are set as follows. At $x = 0$ we set the Dirichlet condition $C = 1$, at $x = 1$ we set the Dirichlet condition $C = 0$, and at the domain edges $y = 0$ and $y = 1$ we set the homogeneous Neumann condition of null concentration flux, which is compatible with the direction of the velocity field. A boundary layer forms in the steady solution at $x = 1$, whose width depends on the value of the viscosity coefficient D.

The computational grids are built by subdividing Ω into a set of regular and equal squares and each square in four equally sized triangles by using the square diagonals.

Four calculations have been performed by considering the following partitionings of the domain in sub-squares: 5×5, 10×10, 20×20 and 40×40. Notice that partitioning Ω with the same number of sub-intervals along the X and Y axis preserves the shape, that is the aspect ratio, of the triangular mesh cells.

The results of each simulation run is given in Table 1. The first column reports the size of the mesh in terms of subdivisions along the X and the Y axis, namely $N_x \times N_y$. The second and third columns give the absolute and relative errors $\mathcal{E}^{abs}$ and $\mathcal{E}^{rel}$ of the cell-averaged concentration with respect to the analytical solution. These errors are measured by using a discrete version of the L^2 norm; that is

$$\mathcal{E}^{abs} = \sqrt{\sum_{i \in \mathcal{T}_h(\Omega)} |\mathsf{T}_i| \, |c_i - C(t, \mathbf{x}_i)|^2} \quad \text{and} \quad \mathcal{E}^{rel}(\mathbf{c}) = \frac{\mathcal{E}^{abs}}{\sqrt{\sum_{i \in \mathcal{T}_h(\Omega)} |\mathsf{T}_i| \, |C(t, \mathbf{x}_i)|^2}}.$$

The fourth column gives the rate of convergence rate measured when the mesh factor h is halved in the mesh refinement process. The next three columns repeat the same information about the linearly-reconstructed vertex concentration. The errors are calculated by similar formulae. All the calculations have been performed by turning off the limiter. It is evident from these results that second-order convergence is attained in nearly all of the runs, thus confirming the theoretical convergence rate. As the viscosity constant takes smaller values, the boundary layer decreases its width. The coarsest grids show the worst resolution as one can expect, and consequently the worst accuracy in the spatial approximation. Nevertheless, by increasing the mesh resolution, the spatial accuracy increases and tends towards the order $\mathcal{O}\left(h^2\right)$, as predicted by the theory.

The steady solutions for different viscosity calculation are shown in Figure 1. When the viscosity constant attains very small values, the limiter is switched on and prevents the formation of numerical oscillations. In this case, however, the mesh resolution is insufficient to define properly a convergence rate, and for this reason we do not show the corresponding error tables.

5. Conclusions

A FV scheme is proposed to solve the time-dependent advection-diffusion equation for the contaminant transport in porous media. The scheme is based on a special limited reconstruction for gradients within cells and at mesh edges. The 2-nd order theoretical convergence rate has been confirmed on a steady model problem, and the method is promising in the numerical simulation of more complex groundwater flow problems.

References

[1] K. W. Morton, Numerical solution of convection-diffusion problems, Chapman & Hall, London, 1996.

[2] V. Casulli, Eulerian-Lagrangian methods for hyperbolic, and convection dominated parabolic problems., in: Computational methods for non-linear problems, Recent Adv. Non-Linear Comput. Mech. 2, 239-269 , 1987.

[3] S. P. Neuman, An Eulerian-Lagrangian numerical scheme for the dispersion-convection equation using conjugate space-time grids, J. Comput. Phys. 41 (2) (1981) 270–294.

[4] C. Dawson, Godunov-mixed methods for advection-diffusion equations in multidimensions, SIAM J. Numer. Anal. 30 (5) (1993) 1315–1332.

[5] C. Dawson, High resolution upwind-mixed finite element methods for advection-diffusion equations with variable time-stepping, Numer. Methods Partial Differential Equations 11 (5) (1995) 525–538.

[6] A. Mazzia, L. Bergamaschi, M. Putti, A time-splitting technique for the advection-dispersion equation in groundwater., J. Comput. Phys. 157 (1) (2000) 181–198.

[7] C. Gallo, G. Manzini, A fully coupled numerical model for two-phase flow with contaminant transport and biodegradation kinetics., Commun. Numer. Methods Eng. 17 (5) (2001) 325–336.

[8] R. Eymard, T. Gallouët, R. Herbin, Finite volume methods, in: Handbook of numerical analysis, Vol. VII, North-Holland, Amsterdam, 2000, pp. 713–1020.

[9] E. Bertolazzi, G. Manzini, A Finite Volume scheme for contaminant transport in porous media, Tech. rep., IAN-CNR (2000).

[10] E. Bertolazzi, G. Manzini, Limiting strategies for polynomial reconstructions in Finite Volume approximations of the linear advection equation, in: In this proceeding, 2002.

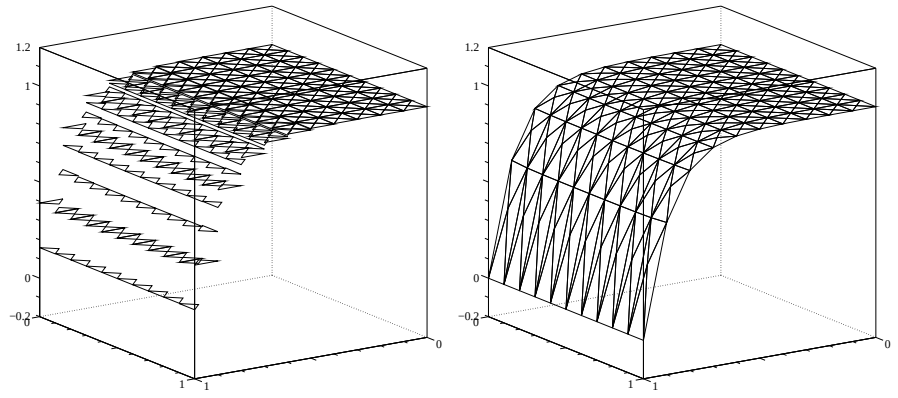

$D = 0.1$

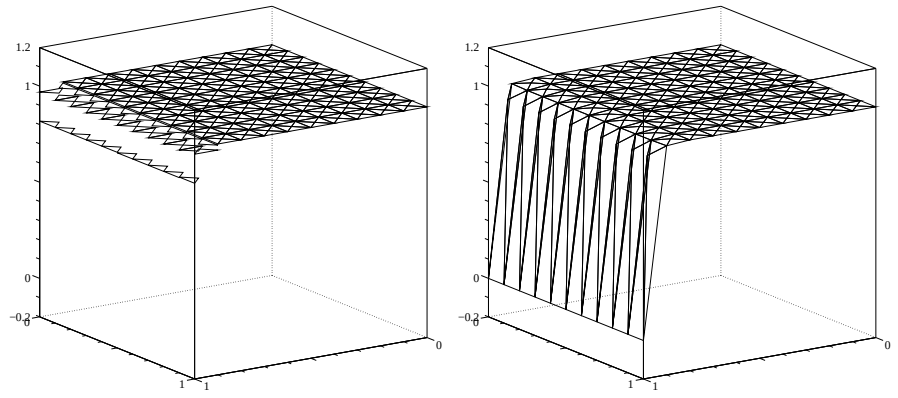

$D = 10^{-2}$

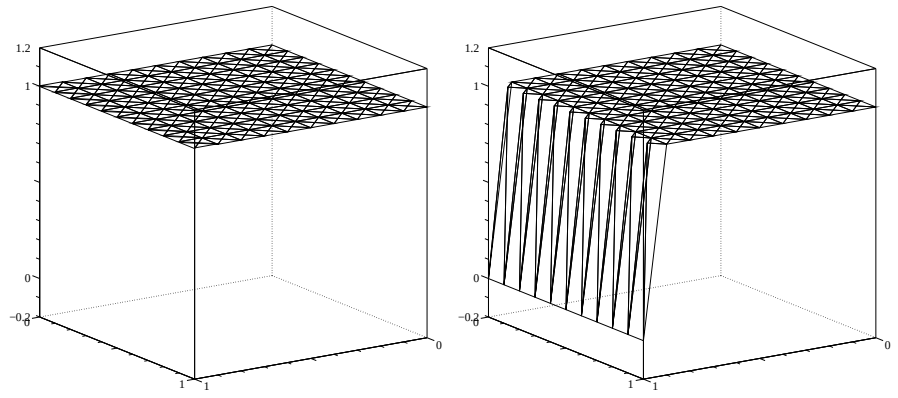

$D = 10^{-4}$

Figure 1: Steady advection-diffusion transport on an unstructured mesh, cell-averaged solution (left) and linearly-reconstructed vertex solution (right) for different viscosity D.